Harmonic Analysis for the Separation of Perfusion and Respiration in Electrical Impedance Tomography

Alberto Battistel * **Rongqing Chen** * **Noël Hallemans** **
Rik Pintelon ** **John Lataire** ** **Knut Möller** *

* *Institute of Technical Medicine (ITeM), Furtwangen University (HFU), Jakob-Kienzle-Strasse 17, 78054 Villingen-Schwenningen, Germany (e-mail: alberto.battistel@hs-furtwangen.de).*
** *Department ELEC, Vrije Universiteit Brussel, Pleinlaan 2, B-1050 Brussels, Belgium*

Abstract:
Electrical Impedance Tomography (EIT) is mainly used to display information about the respiration of a patient. However, also cardiac-related signals are present, and, although they have small amplitude, they can be distinguished by their frequencies. In this contribution, we report a method based on harmonic analysis to separate respiration and perfusion. These are described by a summation of amplitude-modulated signals at different frequencies. We report the mathematical background of the method and its application on the global impedance and, finally, show how it is possible to create frequency-related images highlighting either the respiration or the perfusion inside an EIT video.

Keywords: Electrical impedance tomography; harmonic analysis; respiration and perfusion separation

1. INTRODUCTION

Electrical impedance tomography (EIT) is a routinely performed medical measurement used to follow the respiration of a patient. It is performed injecting small alternating currents around the chest of the patient and recording the associated voltage variations. Since it does require only electric measurements with a relatively small equipment, it is largely employed at the bedside. From the voltage variations an impedance map of a plane of the patient chest is recovered. Because of the inspiration of air in the lungs and their consequent large variation in resistance during the respiration cycle, the main impedance change observed by EIT is associated to the respiration.

However, volume changes, deformation in the heart and shifting of structures within the cardiac cycle are possibly present. Unfortunately their intensity is much lower than that of the respiration (Deibele et al., 2008).

Generally, the combined information about respiration (V) and perfusion (Q) signals will yield an index "V/Q ratio". High V/Q ratios indicate close match between larger volume of inspired air and the perfused blood in the alveoli (Petersson and Glenny, 2014). The V/Q ratio is important for patient under artificial ventilation and it can be used to guide the setting of the ventilator (Putensen et al., 2019).

Several approaches based on principal component analysis with a frequency domain filtering (Deibele et al., 2008) and Gaussian process regression (Graßhoff et al., 2019; Graßhoff and Rostalski, 2020) were proposed for the separation of cardiac-related (perfusion) and respiration components from EIT images. However, because of the large difference in their relative amplitudes and especially because of the superposition of their frequency bands, their separation is not trivial.

Here we propose to take advantage of their difference in base frequencies, that is, in the period of the respiration cycle against the cardiac cycle, to separate the perfusion and respiration. This is undertaken in a post-acquisition elaboration through harmonic analysis analyzing the trend of the EIT signals in the frequency domain.

This method is based on several assumptions: (i) respiration and perfusion can be expressed as a sum of amplitude modulated signals, (ii) the frequencies of respiration and perfusion are stable in the time window of the analysis, (iii) the envelopes of the modulation are smooth enough to be expressed as a low order polynomial, (iv) respiration and perfusion do not share any harmonics, and (v) perfusion and cardiac changes exhibit the same frequency. These assumptions were chosen to make the mathematical problem manageable.

The idea is demonstrated on a series of EIT images taken on a deeply sedated, intubated, and ventilated patient. This guarantees a stable respiration cycle. The mathematical process was first shown on the global impedance and then pixel-wise on a series of EIT images.

⋆ This research was partially funded by BMBF grant number FKZ: 13FH5I05IA COHMED-DigiMed-OP and grant AIRLobe funded by "Innovative Projects" MWK-BW.

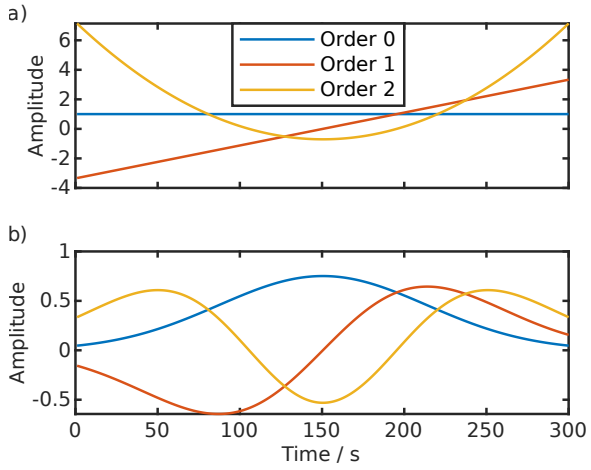

Fig. 1. First orders for shifted Hermite *polynomials* (a) and Hermite *functions* (b).

2. MODEL FOR THE IMPEDANCE VARIATION

Every signal in the impedance tomography, such as the global impedance or the pixel intensity of the EIT images, can be expressed as a time series

$$\mathbf{y} = [y(0)\ y(1)\ \dots\ y(N-1)]^T, \tag{1}$$

where $y(n)$ is shorthand notation for $y(nT_s)$, $T_s = 1/f_s$ is the sampling period, f_s is the sampling frequency and $T = NT_s$ is the measurement time. From assumptions (i)-(ii), this impedance variation can be modelled by

$$y(t) = \sum_{f\in\mathbb{H}} g_f(t)\cos(2\pi ft) - h_f(t)\sin(2\pi ft), \tag{2}$$

where $\mathbb{H}$ is the set of the frequencies consisting of the respiration f_r, the cardiac signal f_p and their harmonics. Under the term harmonics, we understand integer multiples of f_r, f_p and $f_\mathrm{r} - f_\mathrm{p}$. This set of frequencies $\mathbb{H}$ can be estimated from the data using the approach of Pintelon and Schoukens (1996). The functions $g_f(t)$ and $h_f(t)$ represent, respectively, the in-phase and out-of-phase modulations of the frequency f. According to assumption (iii), they can be expressed as

$$g_f(t) = \sum_{p=0}^{N_p} \theta^g_{f,p} b_p(t) \tag{3a}$$

and

$$h_f(t) = \sum_{p=0}^{N_p} \theta^h_{f,p} b_p(t), \tag{3b}$$

with $b_p(t)$, $p = 0, 1, ...$ a complete set of basis functions. Accordingly, from (2) and (3), one writes as a model

$$y(t,\theta) = \sum_{p=0}^{N_p}\sum_{f\in\mathbb{H}} \big(\theta^a_{f,p}\cos(2\pi ft) - \theta^b_{f,p}\sin(2\pi ft)\big) b_p(t), \tag{4}$$

where θ is the parameter vector containing the coefficients $\theta^g_{f,p}$ and $\theta^h_{f,p}$, $f \in \mathbb{H}$ and $p = 0, 1, ..., N_p$. The problem at hand is to estimate the parameters θ from the data $\mathbf{y}$ (1). Knowing the two base frequencies f_r and f_p, it is then possible to relate the different $\theta^a_{f,p}$ and $\theta^b_{f,p}$ to the respiration and to the cardiac dynamics, *de facto* separating their contributions.

Note that in this paper a basis function approach is employed for modelling the smooth functions $g_f(t)$ and $h_f(t)$. An alternative would be to assume that these functions are distributed as a Gaussian process (Rasmussen and Williams, 2006), having the advantage that no model order N_p need to be chosen. The frequency domain approach from Hallemans et al. (2020b) can then be followed.

As a complete set of basis functions $b_p(t)$ in (3), we use shifted Hermite *polynomials* $H_p(x)$,

$$b_p(t) = \pi^{-1/4}2^{p/2}H_p\big(\sqrt{\log 4}\ q(\frac{2t}{T} - 1)\big) \quad t \in [0, T], \tag{5}$$

where q is the same scaling factor used by Boyd and Alfaro (2013). The Hermite polynomials $H_p(x)$ are recursively defined by

$$\begin{aligned} H_0(x) &= 1 \\ H_1(x) &= 2x \\ H_{p+1}(x) &= 2xH_p(x) - 2pH_{p-1}(x). \end{aligned} \tag{6}$$

For the weight function $w(x) = e^{-x^2}$, these possess the orthogonality property

$$\int_{-\infty}^{\infty} w(x)H_p(x)H_r(x)\mathrm{d}x = \sqrt{\pi}2^p p!\delta_{pr}, \tag{7}$$

where δ_{pr} is the Kronecker delta.
In order to reduce spectral leakage, a Gaussian window is applied to the signal, that is

$$y_w(t) = w\Big(\sqrt{\log 4}\ q(\frac{2t}{T} - 1)\Big)y(t). \tag{8}$$

One more time employing the same scaling of Boyd and Alfaro (2013). However, in this formulation, q also works as an adjustable parameter which determines the stretch of the weight function. With $q = 1$ at the sides of the domain the weight function decays by a factor of two. Increasing q, the weight function concentrates more and more at the center of the domain. Accordingly, from (4), it is natural to write

$$y_w(t) = \sum_{p=0}^{N_p}\sum_{f\in\mathbb{H}} \big(\theta^g_{f,p}\cos(2\pi ft) - \theta^h_{f,p}\sin(2\pi ft)\big)\tilde{b}_p(t), \tag{9}$$

where the basis functions $\tilde{b}_p(t)$ turn out to be shifted Hermite *functions* $\Psi_p(x)$

$$\tilde{b}_p(t) = \Psi_p\Big(\sqrt{\log 4}\ q(\frac{2t}{T} - 1)\Big). \tag{10}$$

These derive from the Hermite *polynomials*, including the weight function $w(x)$ in the basis set, and hence, making the functions orthonormal. They are recursively defined by

$$\begin{aligned} \Psi_0(x) &= \pi^{-\frac{1}{4}}e^{-\frac{1}{2}x^2} \\ \Psi_1(x) &= \pi^{-\frac{1}{4}}\sqrt{2}\,xe^{-\frac{1}{2}x^2} \\ \Psi_{p+1}(x) &= \sqrt{\frac{2}{p+1}}\,x\,\Psi_p(x) - \sqrt{\frac{p}{p+1}}\,\Psi_{p-1}(x), \end{aligned} \tag{11}$$

and satisfy the orthonormality condition

$$\int_{-\infty}^{\infty} \Psi_p(x)\Psi_r(x)\mathrm{d}x = \delta_{pr}. \tag{12}$$

In this way, the parameter q is used to control the tapering of the window function. This strategy is employed to

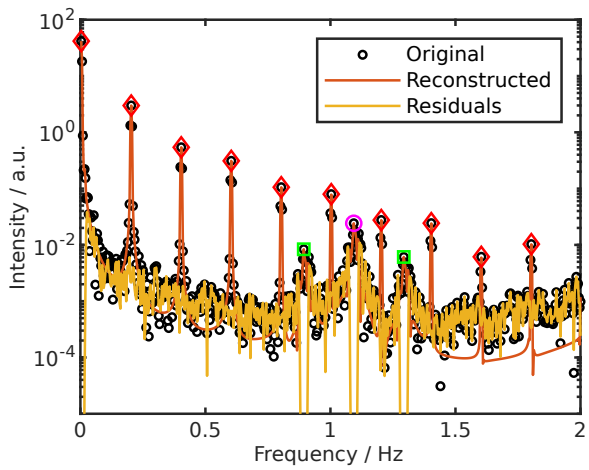

Fig. 2. Fitting of the global impedance in the frequency domain. The red diamond represent the harmonics of the respiration, the violet circle that of the cardiac signal, and the green squares the intermodulations.

control the spectral width of the polynomial modulation in the frequency spectrum.

The first 3 orders for the Hermite *polynomials* and *functions* are displayed in Fig. 1 with a stretching parameter $q = 2$, the same which is used in the following analysis. The *polynomials* have the typical shape of a power series. The Hermite *functions*, instead, decay at the extrema of the time domain because of the Gaussian weight function. Also, they are bounded as $\Psi_n(x) \leq 0.816$ for all n and for all x (Abramowitz and Stegun, 1972) and posses other important properties for fitting, such as an analytical form for their normalization (Boyd and Alfaro, 2013). Moreover, the Hermite *functions* represent the eigenvector of the Fourier transform and, therefore, have the same shape in the time as well as in the frequency domain.

3. A FREQUENCY DOMAIN ESTIMATION APPROACH

To simplify the estimation of the coefficients $\theta^g_{f,p}$ and $\theta^h_{f,p}$, the estimation is performed in the frequency domain. This allows to restrict the time-series data to the frequency band of interest $[0, f_{\max}]$. A similar strategy was already employed by Hallemans et al. (2020a, 2021) to estimate the best linear time-varying approximation (BLTVA) of a certain class of nonlinear time-varying systems.

The time series (1), after windowing (8), is now transformed into the frequency domain using the discrete Fourier transform (DFT)

$$Y_w(k) = \sum_{n=0}^{N-1} y_w(nT_s) e^{-j2\pi nk/N}. \tag{13}$$

Accordingly, the frequency domain data, in the frequency band of interest, is denoted as

$$\mathbf{Y}_w = \left[Y_w(0), Y_w(1), ..., Y_w(F)\right]^T, \tag{14}$$

where $F = \text{ceil}(f_{\max} T)$. The frequency domain model is then obtained by transforming (9) to the frequency domain

$$Y_w(k) = \frac{1}{2} \sum_{p=0}^{N_p} \sum_{f \in \mathbb{H}} (\theta^g_{f,p} - j\theta^h_{f,p}) \tilde{B}_p(k - fT), \tag{15}$$

where $\tilde{B}_p(k)$ is the DFT of $\tilde{b}_p(t)$. Accordingly, the frequency domain data can be rewritten under matrix form

$$\mathbf{Y}_w = K\theta + V, \tag{16}$$

where $\mathbf{Y}_w$ is defined in (14), K is a regression matrix consisting of the basis functions $\tilde{B}_p$ and V is a noise vector. In order to impose that the parameters θ are real, one rewrites the matrix equality (16) as a real-valued one

$$\mathbf{Y}_{w,\text{re}} = K_{\text{re}}\theta + V_{\text{re}} \tag{17}$$

with

$$\mathbf{Y}_{w,\text{re}} = \begin{bmatrix} \text{re}(\mathbf{Y}_w) \\ \text{im}(\mathbf{Y}_w) \end{bmatrix}, K_{\text{re}} = \begin{bmatrix} \text{re}(K) \\ \text{im}(K) \end{bmatrix} \text{ and } V_{\text{re}} = \begin{bmatrix} \text{re}(V) \\ \text{im}(V) \end{bmatrix}. \tag{18}$$

The optimal parameters $\hat{\theta}$ can be obtained in least squares sense

$$\hat{\theta} = \arg\min_{\theta} ||\mathbf{Y}_{w,\text{re}} - K_{\text{re}}\theta||_2^2 \tag{19a}$$

$$= (K_{\text{re}}^T K_{\text{re}})^{-1} K_{\text{re}}^T \mathbf{Y}_{w,\text{re}}. \tag{19b}$$

From the estimated parameter vector $\hat{\theta}$, one then retains the coefficients corresponding to the respiration and perfusion frequencies, and their integer multiples. The separated respiration and perfusion impedances are then, respectively, reconstructed from (4);

$$\hat{y}_{\text{r}}(t) = \sum_{p=0}^{N_p} \sum_{n=1}^{N_h} \big(\hat{\theta}^g_{nf_{\text{r}},p} \cos(2\pi n f_{\text{r}} t) - \hat{\theta}^h_{nf_{\text{r}},p} \sin(2\pi n f_{\text{r}} t)\big) b_p(t) \tag{20a}$$

and

$$\hat{y}_{\text{p}}(t) = \sum_{p=0}^{N_p} \sum_{n=1}^{N_h} \big(\hat{\theta}^g_{nf_{\text{p}},p} \cos(2\pi n f_{\text{p}} t) - \hat{\theta}^h_{nf_{\text{p}},p} \sin(2\pi n f_{\text{p}} t)\big) b_p(t), \tag{20b}$$

where N_h is the number of harmonics. Note that for the regressions matrix K, Hermite *functions* are used, while for the reconstruction in the time domain Hermite *polynomials* are used. In this way, the effect of windowing the data can be removed.

4. METHOD

In this contribution a 5 min long dataset was used. It was sampled at 20 Hz and for image reconstruction GREIT (Adler et al., 2009) was used. The EIT was recorded on deeply sedated, intubated, and ventilated patient before performing a positive end-expiratory pressure (PEEP) step maneuver.

For the harmonic analysis a value of 2 was used for the stretching parameter q, 10 harmonics including the zero frequency were used for the respiration and 2 for the perfusion. For the intermodulation 2 frequencies were considered. $N_p = 15$ coefficients were used for the modulation of the baseline (zero frequency), of the perfusion, and of the intermodulations. A value of $N_p = 2$ was used for all the other components.

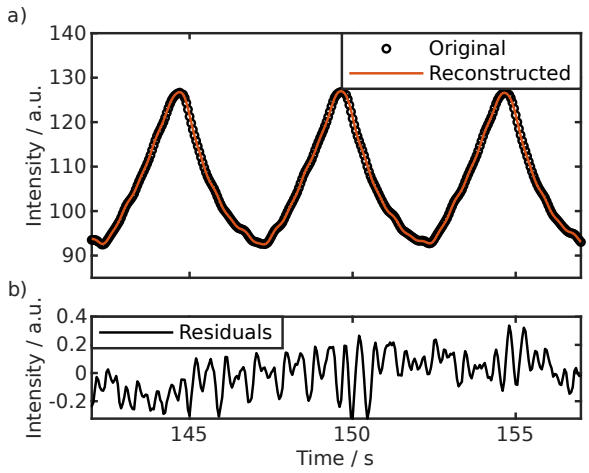

Fig. 3. Global impedance and its reconstruction (a) and residuals (b) in the time domain for a 30 s period.

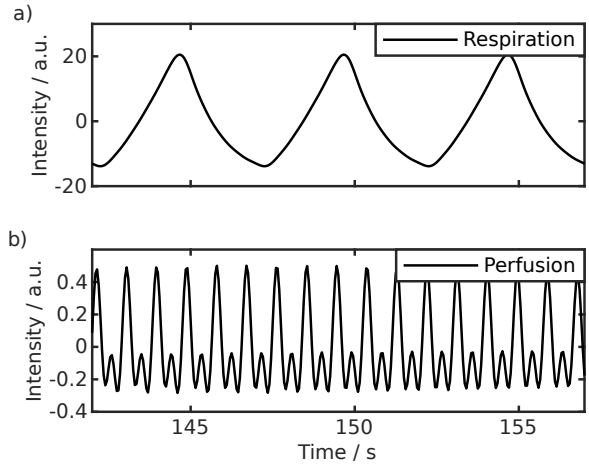

Fig. 4. Reconstructed respiration signal $\hat{y}_{\mathrm{r}}(t)$ (20a) a) and perfusion signal $\hat{y}_{\mathrm{p}}(t)$ (20b) b) from the global impedance.

The harmonic analysis was performed on the global impedance, calculated from the sum of all the pixels of the EIT frames, on the time trend of two distinct pixels, and on all the EIT frames through the use of Principal Components Analysis (PCA). For the PCA, the harmonic analysis was performed on the first 9 principal components which covered more than 99 % of the total variance. After the harmonic analysis, respiration and perfusion were separately reconstructed using (20a) and (20b).

5. RESULTS AND DISCUSSION

Fig. 2 shows the results of the fitting on the global impedance in the frequency band of interest $[0, 2]$ Hz. The respiration had a frequency $f_{\mathrm{r}} = 0.20$ Hz and the heartbeat of $f_{\mathrm{p}} = 1.09$ Hz. The periodic components appear as peaks, the harmonics of the respiration are highlighted by a red diamond while those of the heartbeat by a violet circle (only the first harmonic is visible). The intensity of the first harmonic of the cardiac signal is two orders of magnitude lower than that of the respiration. Also the harmonics of the respiration are very intense even at frequencies higher

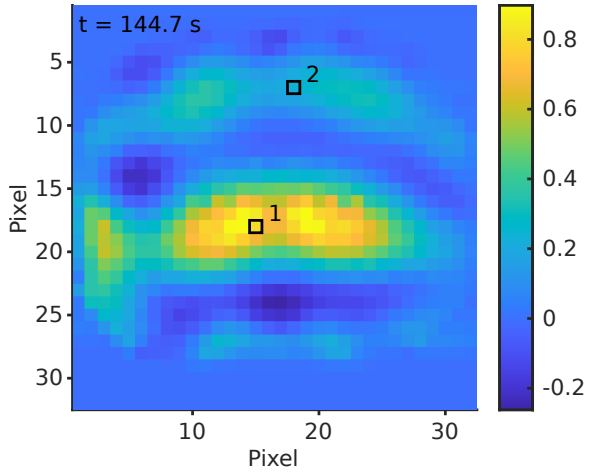

Fig. 5. EIT image at 144.7 s with two pixels highlighted. *Pixel* 1 (15,18) is at a position in the lung area. *Pixel* 2 (18,7) is at the expected position of the heart.

than that of the heartbeat. These two facts explain why it is difficult to effectively separate the perfusion from the respiration in EIT signals.

Interestingly, two additional peaks appeared at *ca.* 0.9 Hz and 1.3 Hz (green squares in Fig. 2), these are the intermodulation of the cardiac signal with the respiration of the patient and represent the modulation of the amplitude of the perfusion given by the respiration or vice versa.

The peaks corresponding to the respiration appear very sharp and well fitted. The peaks of the intermodulation and of the perfusion, instead, are broad and the fitting function could not properly match their shape, as also highlighted by the spectrum of the residuals. This spectrum can be used to estimate the uncertainty on the coefficients $\hat{\theta}^a_{f,p}$ and $\hat{\theta}^b_{f,p}$ recovered by the fitting (Hallemans et al., 2020a, 2021).

Clearly, because of the spectral width of the perfusion signal, which also overlaps with some respiration harmonics, it is not possible to use filtering to decouple respiration and perfusion in EIT.

The difficulty in fitting the perfusion signal was given by the order of the polynomial expansion used to describe the modulation of the periodic signals. However, an arbitrary increase of the order for the perfusion components showed a distortion of the residuals spectrum, indicating a possible overfitting. Note that increasing the order of the modulation polynomial results in a broadening of the peak skirt. Also, even a high order polynomial for the modulation of the perfusion decreased only marginally the sum of squares. This is on one hand in agreement with the low total weight of the cardiac signals in the global impedance. On the other hand, instead, it could be connected with the fact that the perfusion cannot be fully represented by an amplitude modulated signal, as it contains a frequency or phase modulation too.

In Fig. 3 a) the global impedance is compared with its reconstructed function in the time domain, which was reconstructed by using the Hermite polynomials. The two signals show good agreement as also proved by the

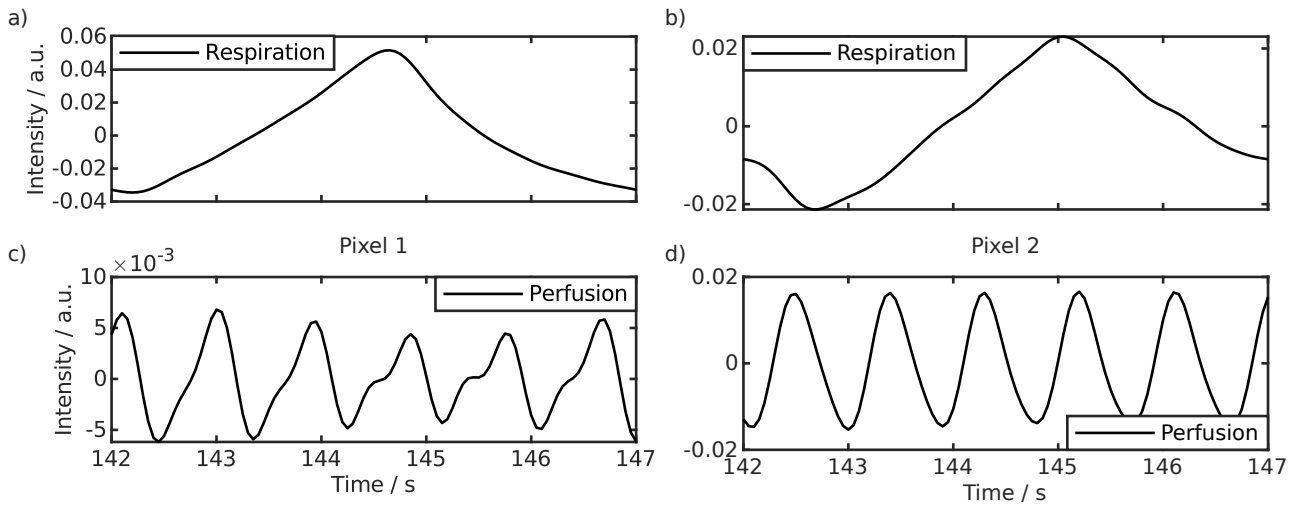

Fig. 6. Reconstructed respiration signals for *Pixel* 1 (a) and for *Pixel* 2 (b) of Fig. 5. Reconstructed respiration signal for *Pixel* 1 (c) and for *Pixel* 2 (d).

magnitude of the residuals in Fig. 3 b) which are more than two orders of magnitude smaller than the global impedance itself.

However, a small quasi-periodic modulation appears in the residuals. This is in agreement with the unfitted width of the cardiac signal in the frequency domain as it is transformed in a spurious quasi-periodic component in time.

The fully separated and reconstructed respiration and perfusion signals are displayed in Fig. 4 a) and b). Note that also the baseline was removed and both signals are plotted around zero.

The respiration had a peak-to-peak intensity of *ca.* 35 while the perfusion of *ca.* 0.65, once more showing the large difference in intensity of the two signals. Also the perfusion has a spiky appearance as that of an electrocardiogram, while the respiration resembles a triangular saw-tooth function.

At the time $t = 144.7\,\mathrm{s}$ both the global impedance and the respiration signal show a maximum which corresponds to the end of the inspiration. An EIT frame for this time instant is reported in Fig. 5. The dorsal area shows an impedance larger than the ventral one. In this frame, two pixels were selected. One corresponding to a position in the lung area (*Pixel* 1) and a second one (*Pixel* 2) at the expected position of the heart.

The harmonic analysis was performed on the time variation of both pixels and the results are reported in Fig. 6. Figure a) and c) show the respiration and perfusion signals for *Pixel* 1, while Figure b) and d) those for *Pixel* 2. Comparing the respiration signals, it is clear that the variation at *Pixel* 1 is larger than that at *Pixel* 2. This is expected since *Pixel* 1 is located in the lung area. However, there is also a difference in the phase of the two signals. In fact, the maximum of the respiration is at two different times: at 144.7 s for *Pixel* 1 and at 145 s for *Pixel* 2.

Similar observations can be made regarding Fig. 6 c) and d). Contrary than for the respiration case, here the

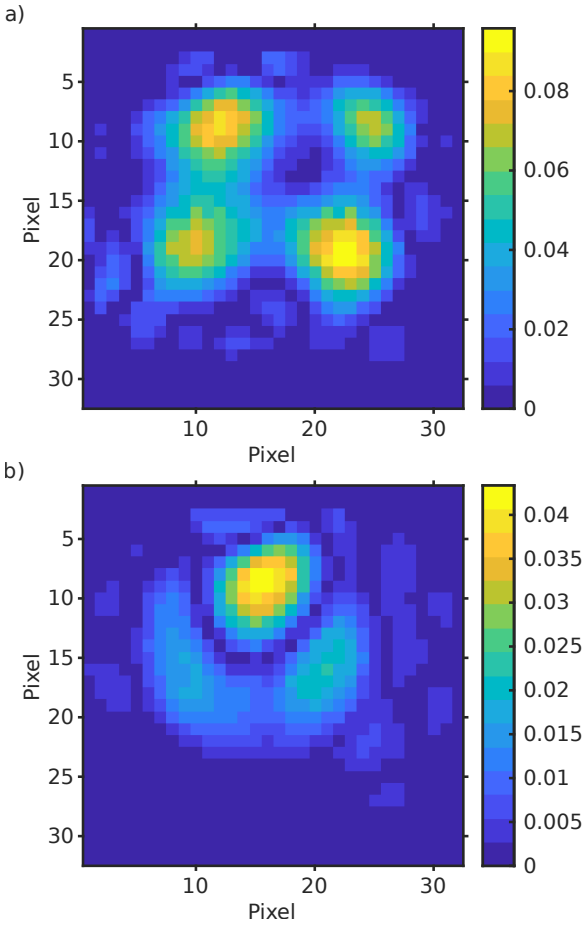

Fig. 7. Respiration (a) and perfusion (b) related EIT images.

perfusion signal is smaller at *Pixel* 1 than at *Pixel* 2. This is in agreement with the assumption that *Pixel* 2 is located in the heart area. Also, the two signals are in phase opposition as at every maximum in Fig. 6 c) corresponds a minimum in Fig. 6 d).

Since for both the respiration and the perfusion signals their amplitude and their phase change at every pixel, it is possible to employ these information to create functional images as in Fig. 7. Fig. 7 a) shows the amplitude of the respiration modulation during the 5 min duration and Fig. 7 b) that of the perfusion. This can be done, for example, extending the same procedure performed on *Pixel* 1 and 2 of Fig. 5 to make the calculate of Fig. 6 to all the other pixels. However, to speed up the computation, the harmonic analysis was applied through the principal components analysis (PCA), in which case a part of the total variance of the signal was lost. This lost was less than 1 % in our case.

Fig. 7 a) shows that the respiration was concentrated on the ventral and dorsal part, but was weak in the middle. Also Fig. 7 a) is substantially different from Fig. 5 where most of the variation in impedance was concentrated at the dorsal area. In Fig. 7 a) instead the regions around pixel (12, 8) and pixel (24,8) were also active with an intensity comparable with the regions of the dorsal part. The rest of the image shows a close-to-zero intensity meaning that the magnitude of the respiration was negligible there.

To derive the same information encoded by Fig. 7 a) one should observe the time variation of the pixel intensity of the EIT map for several minutes.

From Fig. 5 it was not possible to have any information related with the perfusion. This is instead the primary signal in Fig. 7 b), which shows a well defined high intensity region with dark contour at the center of the ventral area. This region can be used to estimate the position of the heart.

This demonstrates how selecting only the frequencies belonging to the respiration or to the perfusion can highlight different aspects of an EIT image.

Finally, amplitudes are positive defined values, which simplifies the scaling of the EIT color bars and chromatics.

Similar as for the amplitude images of Fig. 7 other images can be constructed for the phase of the respiration and of the perfusion signal. These phase related maps have strong contouring capabilities (not shown).

6. CONCLUSIONS

In this contribution we introduced a novel method for the separation of perfusion and respiration signals based on harmonic analysis in EIT images. This approach was based on the assumption that EIT can be decomposed into a combination of amplitude modulated signals. The harmonic analysis was first performed on the global impedance and then pixel-wise on a 5 min long time series. In this way it was possible to construct a respiration-only and a perfusion-only related image. These images highlight the area of maximal amplitude variation of the respiration and of the perfusion and can help to individuate which areas are for example well ventilated or the expected position of the heart.

We foresee that this kind of analysis can simplify the reading of EIT images and support the physician in the judgment of the conditions of the patient. Also since the images are decomposed into amplitude-varying signals it is possible to create fully automatic analysis of the response of the patient to the ventilation.

REFERENCES

Abramowitz, M. and Stegun, I.A. (1972). *Handbook of Mathematical Functions with Formulas, Graphs, and Mathematical Tables*. U.S. Dept. of Commerce, National Bureau of Standards, Washington, D.C.

Adler, A., Arnold, J.H., Bayford, R., Borsic, A., Brown, B., Dixon, P., Faes, T.J.C., Frerichs, I., Gagnon, H., Gärber, Y., Grychtol, B., Hahn, G., Lionheart, W.R.B., Malik, A., Patterson, R.P., Stocks, J., Tizzard, A., Weiler, N., and Wolf, G.K. (2009). GREIT: A unified approach to 2D linear EIT reconstruction of lung images. *Physiological Measurement*, 30(6), S35–S55. doi:10/c2wwft.

Boyd, J.P. and Alfaro, L.F. (2013). Hermite function interpolation on a finite uniform grid: Defeating the Runge phenomenon and replacing radial basis functions. *Applied Mathematics Letters*, 26(10), 995–997. doi: 10/f453v7.

Deibele, J.M., Luepschen, H., and Leonhardt, S. (2008). Dynamic separation of pulmonary and cardiac changes in electrical impedance tomography. *Physiological Measurement*, 29(6), S1–S14. doi:10/c2dp7g.

Graßhoff, J., Jankowski, A., and Rostalski, P. (2019). Scalable Gaussian Process Regression for Kernels with a Non-Stationary Phase. *arXiv:1912.11713 [cs, stat]*.

Graßhoff, J. and Rostalski, P. (2020). Spatio-Temporal Gaussian Processes for Separation of Ventilation and Perfusion Related Signals in EIT Data. *Proceedings on Automation in Medical Engineering*, 1(1), 011–011.

Hallemans, N., Pintelon, R., Zhu, X., Collet, T., Claessens, R., Wouters, B., Hubin, A., and Lataire, J. (2020a). Detection, Classification and Quantification of Nonlinear Distortions in Time-Varying Frequency Response Function Measurements. *IEEE Transactions on Instrumentation and Measurement*, 1–1. doi:10/gj3cjw.

Hallemans, N., Lataire, J., and Pintelon, R. (2020b). Nonparametric identification of linear time-varying systems using gaussian process regression. *IFAC-PapersOnLine*, 53(2), 1001–1006. doi:10/gkrwjq.

Hallemans, N., Pintelon, R., Van Gheem, E., Collet, T., Claessens, R., Wouters, B., Ramharter, K., Hubin, A., and Lataire, J. (2021). Best Linear Time-Varying Approximation of a General Class of Nonlinear Time-Varying Systems. *IEEE Transactions on Instrumentation and Measurement*, 70, 1–14. doi:10/gk9bpw.

Petersson, J. and Glenny, R.W. (2014). Gas exchange and ventilation–perfusion relationships in the lung. *European Respiratory Journal*, 44(4), 1023–1041. doi: 10/f247pw.

Pintelon, R. and Schoukens, J. (1996). An improved sine-wave fitting procedure for characterizing data acquisition channels. *IEEE Transactions on Instrumentation and Measurement*, 45(2), 588–593. doi:10/bg9qp5.

Putensen, C., Hentze, B., Muenster, S., and Muders, T. (2019). Electrical Impedance Tomography for Cardio-Pulmonary Monitoring. *Journal of Clinical Medicine*, 8(8), 1176. doi:10/gg782m.

Rasmussen, C.E. and Williams, C.K.I. (2006). *Gaussian Processes for Machine Learning*. MIT press.